Laser and Particle Beams (2007), *25*, 613–620. Printed in the USA.

DOI: 10.1017/S0263034607000729

Saturation effect at high laser pulse energies in laser-induced breakdown spectroscopy for elemental analysis in water

XIAO FANG AND S. RAFI AHMAD
Centre for Applied Laser Spectroscopy, DMAS, DCMT, Cranfield University, Shrivenham, Swindon, United Kingdom
(RECEIVED 5 May 2007; ACCEPTED 1 September 2007)

Abstract

Saturation effects in laser-induced breakdown spectroscopy in water for elemental analysis have been investigated. Existing theoretical model of laser-induced plasma in solids has been applied to liquid phase under some simplifying assumptions to take account of the laser pulse energy dependence of atomic emissions from Na and Cu in aqueous solution. The theory was found to explain the emission process for laser energies up to but below the saturation level. The saturation limit of the emission with laser pulse energy corresponds well with that of the plasma temperature deduced from blackbody emission considerations. The saturation energies for atomic emissions were found to be lower for bulk excitations compared to water jet excitations. The dependence of signal strength on sample concentration indicated that the concentration values at saturation are lower at higher laser energies, as is expected from the theoretical model.

Keywords: Atomic Emission; Laser; Plasma Temperature; Saturation; Water Plasma

INTRODUCTION

High-power lasers are now widely used for a variety of applications (Abdallah *et al.*, 2007; Bashir *et al.*, 2007; Schaumann *et al.*, 2005; Schollmeier *et al.*, 2006; Wolowski *et al.*, 2007). Due to the technological development they are used as atomization tools in atomic spectroscopy of solid samples for elemental analysis (Ciucci *et al.*, 1999; Schade *et al.*, 2006; Thareja & Sharma, 2006). The use of lasers in place of other thermal sources allows in situ, non-invasive and remote monitoring, and analysis of species in inaccessible or hazardous locations (Whitehouse *et al.*, 2001). However, the prospect of using a laser-based atomic spectrometer for in situ elemental analysis in water environment without the need for any sample preparation protocol, and an expert operator has prompted a spate of research initiatives in recent time. The scope of such research has been quite diverse and the main emphasis has been put on signal-to-noise ratio (S/N) improvement, the noise being contributed primarily by the shot noise component of the white Brehmsstrahlung emission from the plasma of the host water molecules. Effects of laser parameters such as wavelength (Whitehouse *et al.*, 2001) and pulse energy (Cabalin & Laserna, 1998), and experimental conditions such as double-pulse excitation (St-Onge *et al.*, 2002), signal detection methodology (Detalle *et al.*, 2001), and sample presentation geometry (Samek *et al.*, 2000) on the S/N have been reported. Despite the diversity of experimental parameters and conditions, there is a general consensus as to the feasibility of monitoring trace elements in water using laser induced breakdown spectroscopy (LIBS), although the optimum experimental parameters for this technique are yet to be defined.

The saturation of atomic emission intensity in plasma inherently limits the laser fluence that can be used for optimizing detection sensitivity. The saturation phenomenon is well documented (Bauerle, 1996) for solid samples and is explained in terms of a dynamic equilibrium between laser energy absorption and plasma expansion and consequent cooling. In water, this dynamic process will depend on both the environment of the plasma as well as laser and material parameters. While fluence dependence of Na emission intensity in water jet (air being the plasma environment) has been studied (Charfi & Harith, 2002), no comparison of the saturation limit of plasma emission in the bulk (water environment) and on surface (or jet) excitations has so far been reported in the literature.

Although theoretical models for dynamical processes of laser interaction in solids, leading to a state of saturation do exist, such models are not strictly applicable for liquid

Address correspondence and reprint request to: Xiao Fang, Centre for Applied Laser Spectroscopy, DMAS, DCMT, Cranfield University, Shrivenham, Swindon, Wilts. SN6 8LA, United Kingdom. E-mail: x.fang@cranfield.ac.uk

samples. A rigorous theoretical analysis of the dynamics of high-power laser interaction process in liquid is beyond the scope of this paper. However, a phenomenological approach, based on the model developed for solid-phase interaction and some simplifying assumption, may give a plausible explanation of the observed results on saturation of emission at relatively high laser fluence and the concentration of the atomic species.

THEORETICAL BASIS

The intensity of an emission line, $I_{nm,}$ due to an electronic transition between two states, $m \rightarrow n$ $(n > m)$ is governed primarily by the plasma temperature dependence through the Boltzman factor (Bauerle, 1996) and is expressed as follows:

$$I_{nm} = G(hc/\lambda_{nm})(g_i A_i/Z)N_s \ \mathrm{Exp}(-E_n/kT), \tag{1}$$

where G is the instrumental constant, h is the Plank's constant, c is the speed of light, λ_{nm} is the wavelength value of the emission line, g_i is the statistical weighting factor, A_i is the Einstein's spontaneous emission coefficient, Z is the partition factor, N_s is the population of the target species within the plasma volume, E_n is the energy of the upper state (n), k is the Boltzman constant, and T is the plasma temperature.

The theory assumes a local thermodynamic equilibrium. In this, the dissipation of laser deposited energy within the duration of a short laser pulse is neglected. For the evaluation of a general trend on the dependence of emission intensity on the plasma temperature, the contribution of temperature dependence of the partition function could be ignored (Bassiotis *et al.*, 2001), so that Eq. 1 could be expressed in terms of plasma temperature dependent parameters only as:

$$I_{nm} = K_1 \mathrm{Exp}(-E_n/kT), \tag{2}$$

where the assumed temperature independent term, $K_1 = G(hc/\lambda_{nm})(g_i A_i/Z)\ N_s$.

The modeling of temporal temperature profile in solids due to pulsed laser heating is a complex procedure, involving several dynamic and kinetic photo-physical and photochemical processes. Despite this, modeling currently carried out using a stochastic approach and drastic simplifying assumptions on temperature dependence of optical properties of the material has given satisfactory results (Houle & Hinsburg, 1998). We may consider the conventional heat equation relating the temporal evolution of the temperature with the competitive processes of heat input and redistribution within the heated volume as:

$$\rho C_p(T)\delta T/\delta t = H + \nabla \cdot (K(T)\nabla T), \tag{3}$$

where T is a function of space (x, y, z) and time (t), H is a heat source term in units of power per unit volume, $K(T)$ is the temperature dependent thermal conductivity, $\rho = n/V$ is the density of the material (moles/volume), and $C_p(T)$ is the temperature-dependent heat capacity. Volume integral of the above equation can be written as:

$$nC_p\delta T/\delta t = kQ + K(T)T, \tag{4}$$

where k is the rate constant for energy input and Q is the energy content within the volume. For nanosecond laser pulses, the temperature rise to its maximum value, for the present purposes, could be assumed to be instantaneous, so that:

$$nC_p T_{max} = P_{abs} + K(T)T_{max}, \tag{5}$$

where T_{max} is the maximum temperature, P_{abs} is the absorbed power density ($\mathrm{J.cm^{-2}.s^{-1}}$), and is given by Beer's law as:

$$P_{abs} = P_i(1 - R(T))\mathrm{Exp}(-\alpha(T)d), \tag{6}$$

where P_i is the incident power density, $R(T)$ is the temperature dependant reflectivity of the laser irradiated volume, $\alpha(T)$ is the temperature dependent absorption coefficient and d is the length parameter of the heated volume.

From Eqs. 5 and 6, a relation between the maximum incident laser power density and the maximum temperature rise can be obtained by a phenomenological argument that the maximum temperature corresponds to the maximum absorbed power density and is assumed to be instantaneous. Under the simplifying assumptions, expected to be valid before the saturation limit, the reflectance, thermal conductivity, and the absorption coefficient terms could each be represented by an average value. Therefore, from Eqs. 2, (5), and (6):

$$I_{nm} = K_1 \mathrm{Exp}(-E_n/K_2 P_i),$$

that is,

$$\ln(I_{nm}) = (-E_n/K_2) \times \tau/E_l + \ln(K_1), \tag{7}$$

where the constant $K_2 = k(nC_p - K) = k(N_A N_s V C_p - K)$, $N_A =$ Avagadro's number, V is the volume of the sampled region, N_s is the number of target species within the plasma volume, τ is the laser pulse duration, and E_l is the incident laser intensity.

EXPERIMENTAL DETAILS

The experimental setup shown schematically in Figure 1, consists of a laser source, a sample presentation system, a monochromator/spectrograph, and the choice of two detection systems, one based on an intensified diode array/optical multichannel analyzer, and the other on photomultiplier/gated charge integrator. The latter was used in this

https://doi.org/10.1017/S0263034607000729 Published online by Cambridge University Press

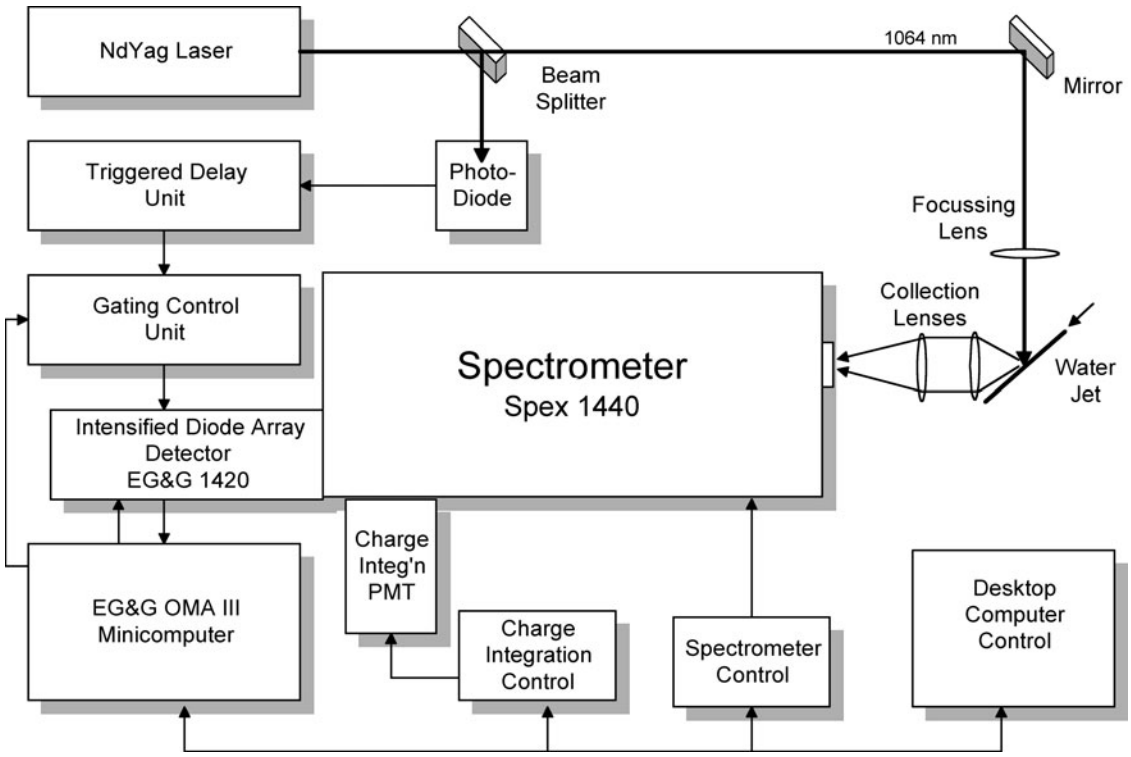

Fig. 1. Schematic of apparatus for laser induced breakdown spectroscopy experiments in water for elemental analysis.

experiment as it allowed suitable variable gate pulse and gate width to be applied in signal detection, and also this gave comparatively better S/N ratio.

The laser source is Nd-YAG (Litron 200-UK), operating at 1064 nm wavelength and capable of delivering a maximum energy of 200 mJ over a pulse duration of ~ 6 ns (FWHM) at a maximum pulse repetition rate of 20 Hz. The beam diameter at the exit is 5 mm and the quoted beam divergence is <2 mrad. A 25 mm focal length lens was used to focus the beam on to the water sample.

The spectral dispersion was achieved by a high-resolution (maximum $\sim 10\ \mathrm{cm}^{-1}$) f/7.8 double monochromator (SPEX 1404). The spectral purity is quoted to be $<10^{-14}$ at wavelength >0.5 nm from a set wavelength. The spectral coverage extends from UV to near IR wavelengths depending upon the grating type being used. The plasma source was imaged on to the entrance slit of the monochromator with a combination of a collecting lens and a focusing lens, giving an *f*-number nearly matching that of the monochromator.

Temporal scans of the emission from plasma and the laser were recorded using a digital oscilloscope (Digiscope-HP5411D-HP). The bandwidth of the instrument was 500 MHz, thus enabling it to faithfully reproduce signals with rise time of ≥ 2 ns. The gated charge integrator electronic system (EG&G Model 4420) allowed detection of signals from the plasma through a time gate of width, variable between 2 ns to 2 ms after a time delay from the laser pulse, variable from a minimum of 50 ns (even at zero setting) to 10 μs. The photomultiplier (electron Tube-9214B) has a rise time of 2 ns and a spectral window for good response of 300–600 nm.

For sample presentation, a water jet system incorporating a pump and an interchangeable nozzle attachment was used. The nozzle was tapered to give a laminar flow of water having a cross section of approximately 0.5 mm × 2 mm. The sample was circulated through the system at a flow rate of 0.5 l/min. Because of the problem of water contamination on the surface of the focusing lens it was necessary to confine the jet within a metal container with a hole for focusing the laser beam on to the jet.

RESULTS AND ANALYSIS

Laser Pulse Energy Dependence

The laser pulse energy values were selected by varying the high voltage to the flash lamp at the control panel of the laser power supply. For aqueous samples of sodium (Na) at a concentration of 10 ppm and copper (Cu) at 300 ppm, the signal intensities of atomic emission from laser induced plasmas at 589 nm and 324.7 nm and the background noise were measured respectively and the signal-to-noise ratios (S/N) against exciting laser energy are shown in Figure 2. Each data point is an average of

https://doi.org/10.1017/S0263034607000729 Published online by Cambridge University Press

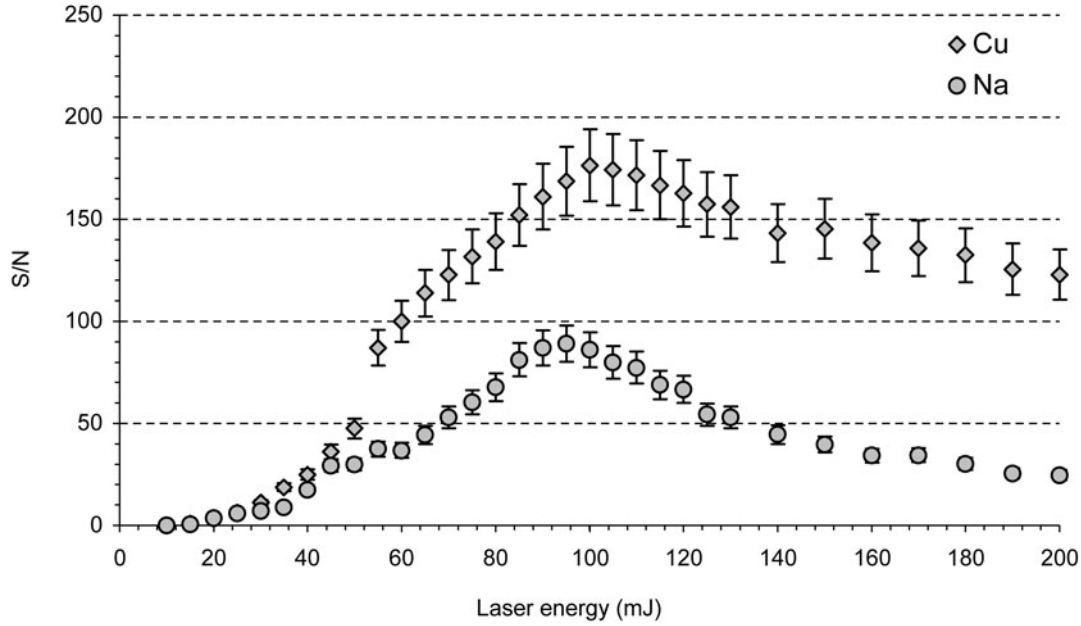

Fig. 2. Plots of S/N versus laser pulse energy for Na (589 nm) and Cu (324.7 nm) lines in a water jet sample presentation configuration.

80 laser shots at a pulse repetition rate of 20 Hz and the time gate width and delay were set as 10 μs and 2 μs, respectively, for the water jet sample presentation configuration. The signal intensity was found to increase exponentially with laser pulse energy until saturation level. The contribution from the broadband noise was found to increase relatively slowly with the laser energy up to and beyond the signal saturation level. These combined effects gave well-defined values of maximum laser energy for optimum S/N as ∼95 mJ for Na and ∼100 mJ for Cu. Similar measurements were also carried out, where the sample was irradiated with a focused laser beam in to the bulk of the sample, and the spectral signals were acquired with the time gate width and delay of 2 μs and 0.2 μs, respectively. The plasma thus created within the water bulk gave

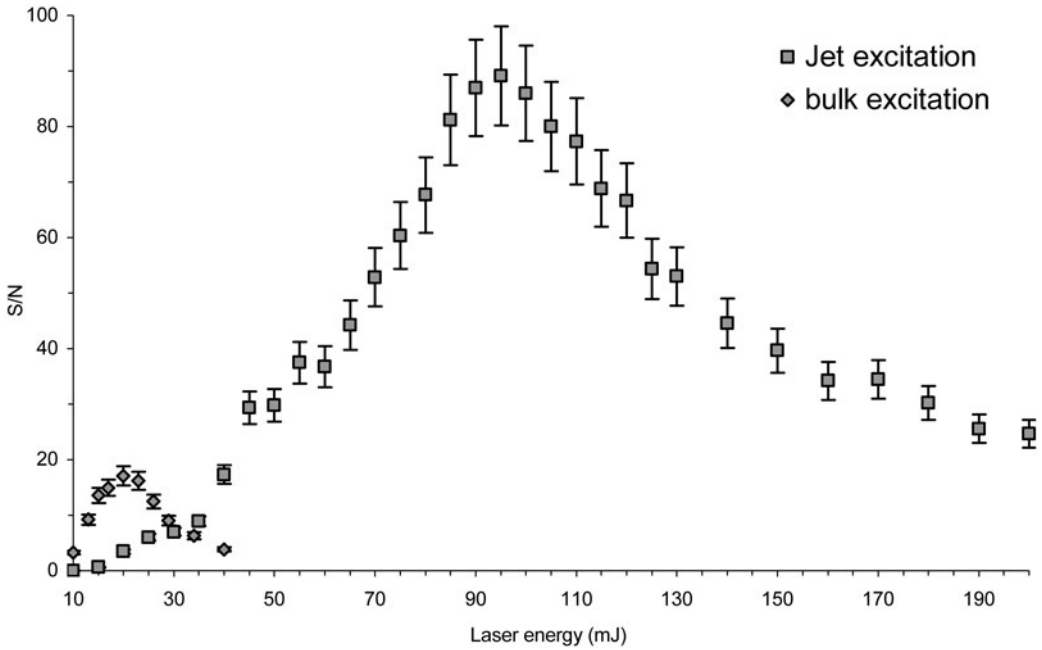

Fig. 3. Plots of S/N versus laser pulse energy for Na line (589 nm) when the plasma was produced in water bulk and on jet surface.

https://doi.org/10.1017/S0263034607000729 Published online by Cambridge University Press

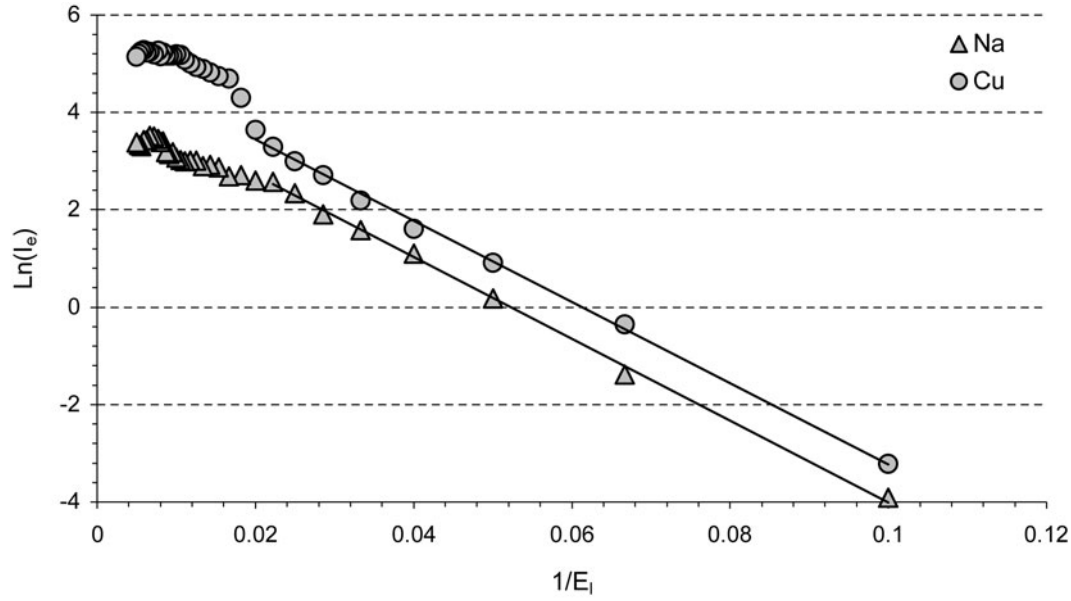

Fig. 4. Plot of logarithm of the emitted intensity of the Na line (589 nm) versus inverse laser pulse energy (see Eq. 7).

comparatively much lower saturation values, e. g. ~20 mJ and ~30 mJ for the Na and Cu lines, respectively, but with S/N lower than that for the water jet sample presentation configuration. The results obtained by bulk excitation and water jet excitation for Na is shown in Figure 3 for comparison.

To validate the theoretical model relating the dependence of emitted intensity from the target species on laser energy, as given in Eq/ (7), ln (I_e) was plotted against $1/E_l$, where I_e is the background corrected emitted intensity and E_l is the laser energy, as shown in Figure 4. The experimental conditions such as time gate delay and width were the same as those for Figure 2. It is reasonable to expect that the derivation of Eq. 7 may be valid at least for values of laser energies below the saturation level. On this basis, a straight line was fitted to the data points. This appears to deviate from the linearity above 40 ± 10 mJ for both Na (at 589 nm) and Cu

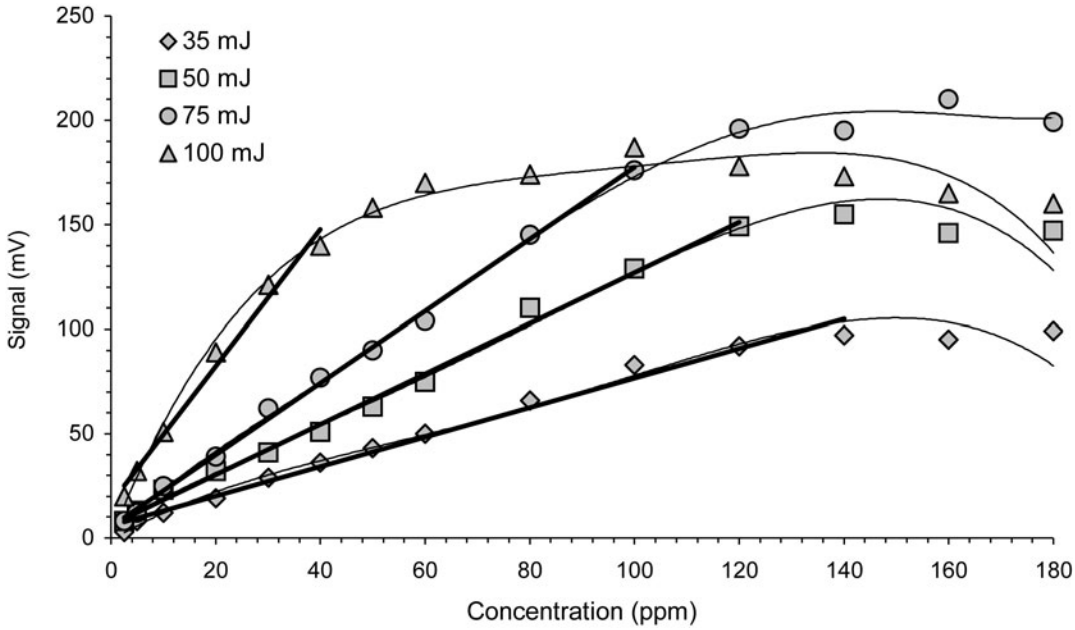

Fig. 5. Plot of emitted signal intensity of Na line (589 nm) versus its concentration in water with laser pulse energy as a parameter.

https://doi.org/10.1017/S0263034607000729 Published online by Cambridge University Press

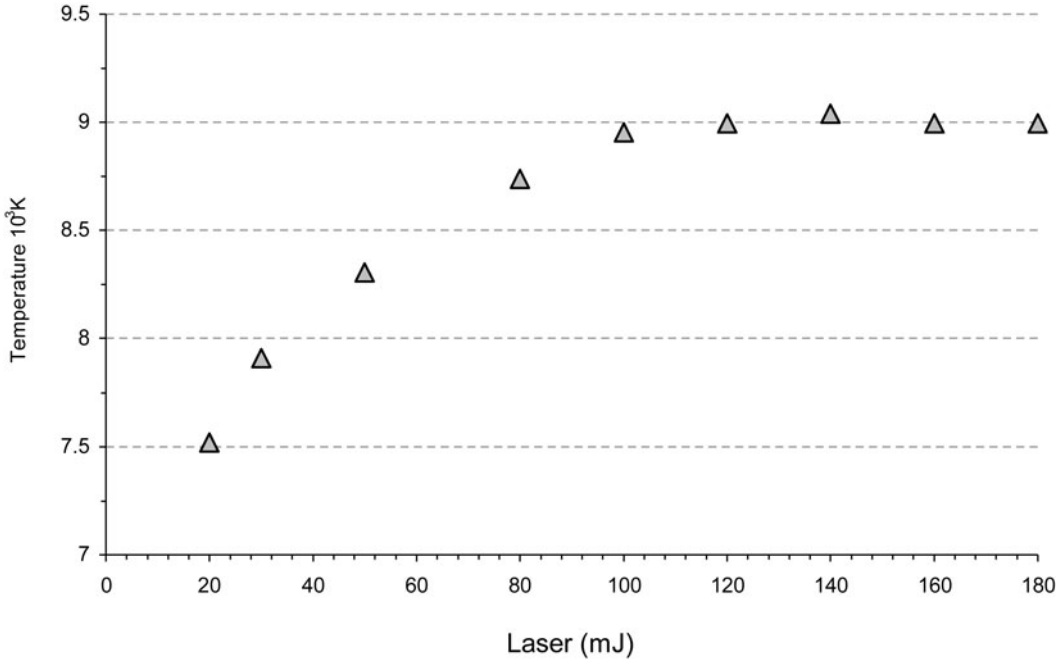

Fig. 6. Plot of plasma temperature deduced from the blackbody emission concept versus laser pulse energy.

(at 324.7 nm) lines, indicating that the model is valid for the lower values of laser energies, at least for the region of exponential rise of the intensity.

Species Concentration Dependence

The intensities of the emitted Na line were measured for different concentrations of Na atoms in an aqueous solution of NaCl salt, over a range of 3–180 ppm. Similar measurements were carried out for four different values of the laser energy, keeping all experimental parameters the same. The signal intensities (in arbitrary units) were plotted against concentration as shown in Figure 5. For lower values of concentrations, the data points fit straight lines and exhibit non-linearity at higher values of target species concentrations. From the fitted straight lines, values of saturation limits for laser pulse energy could be estimated.

DISCUSSION AND CONCLUSIONS

In the literature (Charfi & Harith, 2002), the laser pulse energy at saturation for the S/N for the detection of Na

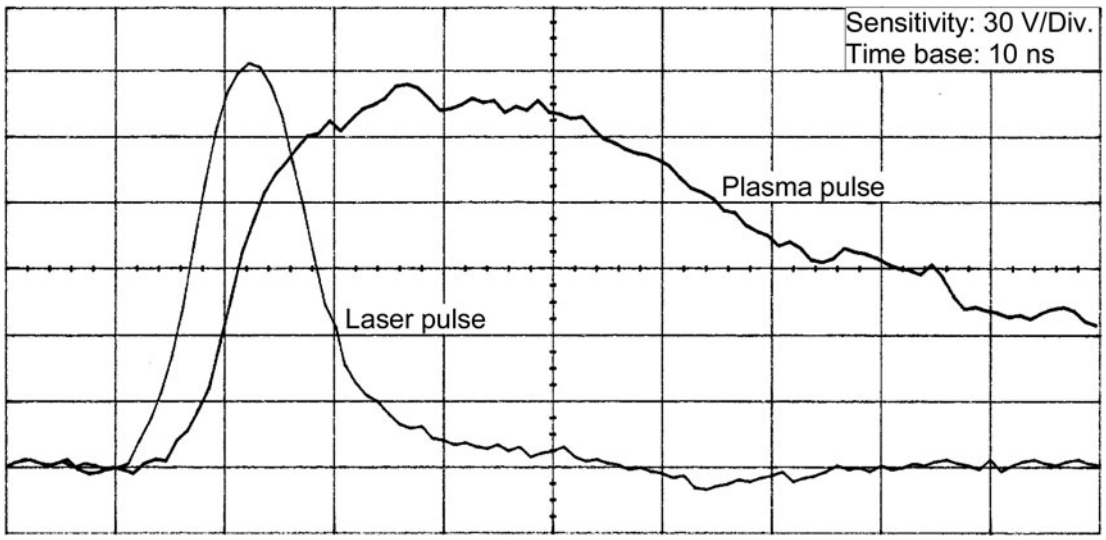

Fig. 7. Temporal profiles of the laser pulse and the corresponding plasma emission pulse.

https://doi.org/10.1017/S0263034607000729 Published online by Cambridge University Press

lines (589 nm and 589.6 nm) was ~96 mJ. Under similar experimental conditions (laser wavelength, sample presentation configuration, etc.) but at a different Na concentration and focused volume, the saturation energy obtained in the present measurement was found to be 93 mJ. A similar observation has been made for the emission from Cu having a saturation value of ~105 mJ i.e., the same as that for the Na line. It is to be noted that the saturation level is also strongly dependent on the nature of emission, i.e., atomic or ionic, as well as on the wavelength of emission.

The temperature rise and the formation of plasma due to electron-ion collision in water medium is a dynamic process. It involves evaporation, atomization/ionization (plasma formation), plasma expansion, plasma heating, and the subsequent emission from the target atoms and ions as well as Brehmsstrahlung emission, plasma expansion and the consequent cooling. The process has not yet been fully understood or modeled satisfactorily. From phenomenological considerations, it can be argued that the emission intensity from the target species and the electron density in the plasma will be functions of the plasma temperature. However, at higher electron densities proportionately increased absorption of the emitted signal from the target species (self absorption) will take place, thus giving rise to a saturation level. Assuming a local thermodynamic equilibrium during the fast laser heating, the plasma can be considered to be a blackbody radiator. From the spectral signatures of the water plasma emission, the maximum wavelength of emission was evaluated and the plasma temperature was calculated from the Wein's displacement law (Plank's radiation law). The plasma temperatures, thus determined, were plotted against laser pulse energy as shown in Figure 6. It is noted that the gated integrator used for the present experiment had an inherent gate delay (as mentioned above) of ~50 ns. Therefore, the temperature that is estimated is not the maximum value corresponding to the peak of the laser pulse, but a value after ~50 ns from the maximum value. At this delay, the plasma temperature may drop down to approximately half of its initial value. This may be inferred from temporal profiles of the laser pulse and the plasma emission pulse simultaneously as shown in Figure 7, and assuming that the emission decay will faithfully follow the decrease in plasma temperature. Plasma temperature, calculated from the emission lines of Ca and the Saha's equation, has also been found (Knop *et al.*, 1996) to show a trend similar to that observed in the temporal history of the plasma decay in Figure 7, albeit at an excitation wavelength of 308 nm.

The inherent saturation of atomic emission in laser-induced plasma imposes an upper limit of the laser energy that can be used for maximum S/N. The saturation value depends on the emission wavelength, being higher for shorter wavelengths, on the environment of the plasma, i.e., lower for water (bulk excitation) compared to air (jet excitation), in addition to its dependence on the nature of emission, i.e., ionic or atomic. The theoretical model of laser initiated temperature rise in solids can be applied, under some simplifying assumptions, to account for the temperature rise in liquid only up to the saturation level. The concentration term, N_s, appears in the wavelength independent constant terms, K_1 and K_2 (Eq. 7), one showing a direct dependence and the other providing an exponential decrease. The laser energy term appears within the exponential term and the saturation level is expected at lower concentrations at higher laser energies. However, the theory, at this stage, could not be applied to deduce quantitative information or validation of the model.

REFERENCES

Abdallah, J., Batani, D., Desai, T., Lucchini, G., Faenov, A., Pikuz, T., Magunov, A. & Narayanan, V. (2007). High resolution X-ray emission spectra from picosecond laser irradiated Ge targets. *Laser Part. Beams* **25**, 245–252.

Bashir, S., Rafique, M.S. & Ul-Haq, F. (2007). Laser ablation of ion irradiated CR-39. *Laser Laser Part. Beams* **25**, 181–191

Bassiotis, I., Diamantopoulou, A., Giannoudakos, A., Roubani-Kalantzopoulou, F. & Kompitsas, M. (2001). Effects of experimental parameters in quantitative analysis of steel alloy by laser-induced breakdown spectroscopy. *Spectrochemica Acta* **B56**, 671–683.

Bauerle, D. (1996). *Laser Processing and Chemistry*. New York: Springer-Verlag.

Cabalin, I.M. & Laserna, J.J. (1998). Experimental determination of laser induced breakdown thresholds of metals under nanosecond Q-switched laser operation. *Spectrochimica Acta* **B53**, 723–730.

Charfi, B. & Harith, M.A. (2002). Panoramic laser-induced breakdown spectroscopy of water. *Spectrochemica Acta* **B57**, 1141–1153.

Ciucci, A., Palleschi, V., Rastelli, S., Salvetti, A., Singh, D.P. & Tognoni, E. (1999). CF-LIPS: A new approach to LIPS spectra analysis. *Laser Part. Beams* **17**, 793–797.

Detalle, V., Heon, R., Sabsabi, M. & St-Onge, L. (2001). An evaluation of a commercial Echelle spectrometer with intensified charge-couple device detector for material analysis by laser-induced plasma spectroscopy. *Spectrochemica Acta* **B56**, 1011–1025.

Houle, F.A. & Hinsburg, W.D. (1998). Stochastic simulation of heat flow with application to laser–solid interactions. *Appl. Phys.* **A66**, 143–151.

Knop, R., Scherbaum, F.J. & Kim, J.I. (1996). Laser induced breakdown spectroscopy (LIBS) as an analytical tool for the detection of metal ions in aqueous solutions. *Fresenius J. Anal. Chem.* **355**, 16–20.

Samek, O., Beddows, D.C.S., Kaiser, J., Kukhlevsky, S.V., Liska, M., Telle, H.H. & Young, J. (2000). Application of laser-induced breakdown spectroscopy to in situ analysis of liquid samples. *Opt. Eng.* **39**, 2248–2262.

Schade, W., Bohling, C., Hohmann, K. & Scheel, D. (2006). Laser-induced plasma spectroscopy for mine detection and verification. *Laser Part. Beams* **24**, 241–247.

Schaumann, G., Schollmeier, M.S., Rodriguez-Prieto, G., Blazevic, A., Brambrink, E., Geissel, M., Korostiy, S., Pirzadeh, P., Roth, M., Rosmej, F.B., Faenov, A.Y., Pikuz, T.A., Tsigutkin, K., Maron, Y., Tahir, N.A. & Hoffmann, D.H.H. (2005). High

https://doi.org/10.1017/S0263034607000729 Published online by Cambridge University Press

energy heavy ion jets emerging from laser plasma generated by long pulse laser beams from the NHELIX laser system at GSI. *Laser Part. Beams* **23**, 503–512.

Schollmeier, M., Prieto, G.R., Rosmej, F.B., Schaumann, G., Blazevic, A., Rosmej, O.N. & Roth, M. (2006). Investigation of laser-produced chlorine plasma radiation for non-monochromatic X-ray scattering experiments. *Laser Part. Beams* **24**, 335–345.

St-Onge, L., Detalle, V. & Sabsabi, M. (2002). Enhanced laser-induced breakdown spectroscopy using the combination of fourth-harmonic and fundamental Nd-YAG laser pulses. *Spectrochemica Acta* **B57**, 121–135.

Thareja, R.K. & Sharma, A.K. (2006). Reactive pulsed laser ablation: Plasma studies. *Laser Part. Beams* **24**, 311–320.

Whitehouse, A.I., Young, J., Botheroyd, I.M., Lawson, S., Evans, C.P. & Wright, J. (2001). Remote material analysis of nuclear power station steam generator tubes by laser-induced breakdown spectroscopy. *Spectrochimica Acta* **B56**, 821–830.

Wolowski, J., Badziak, J., Czarnecka, A., Parys, P., Pisarek, M., Rosinski, M., Turan, R. & Yerci, S. (2007). Application of pulsed laser deposition and laser-induced ion implantation for formation of semiconductor nano-crystallites. *Laser Part. Beams* **25**, 65–69.